Available online at www.sciencedirect.com
SCIENCE DIRECT®
Geochimica et Cosmochimica Acta 70 (2006) 2253–2263
Geochimica
www.elsevier.com/locate/gca

The role of citrate and phthalate during Co(II) coprecipitation with calcite

Young J. Lee *, Richard J. Reeder

Department of Geosciences and Center for Environmental Molecular Science, State University of New York at Stony Brook, Stony Brook, NY 11794-2100, USA

Received 30 September 2005; accepted in revised form 25 January 2006

Abstract

The influence of citrate and phthalate on Co coprecipitation with calcite was investigated using a combination of batch experiments, Fourier-transform infra-red (FT-IR) spectroscopy, and thermogravimetric analysis (TGA) over a wide range of precipitation rates. Steady-state growth conditions (at constant [Ca], [Co], DIC, and pH) were generally achieved within 3–5 h, after which Co(II) partitioning into calcite was evaluated. Only minor differences are observed in the partition coefficient (K_d) trends with and without citrate and phthalate as a function of calcite precipitation rate except at very low rates. Slight inhibition of calcite growth is observed in the presence of citrate or phthalate, which can be attributed to adsorption at surface sites. TGA curves for samples coprecipitated with citrate show a significant mass loss between 375 and 550 °C, whereas the weight-loss curves for the Co–phthalate coprecipitates are indistinguishable from those of the organic-free Co coprecipitates. This indicates that citrate is incorporated into calcite during calcite crystallization, whereas phthalate is excluded. FT-IR spectra for the sample with citrate show a broad absorption in the range 3700–3100 cm^{-1}, which is attributable to water molecules coordinated to citrate coprecipitated with calcite. The preferential incorporation of citrate over phthalate likely reflects differences in both aqueous speciation and conformation of the carboxylate groups. This new finding may provide new insight to the factors that control the behavior of macromolecules and their incorporation into the structure of calcium carbonate during biomineralization.

1. Introduction

Metal partitioning into calcite has been shown to be effective in sequestration of many trace metals in natural and contaminated systems (Mucci and Morse, 1990; Rimstidt et al., 1998; Curti, 1999). As a consequence, metal interactions at the calcite–water interface may be of great importance in influencing the fate and transport of trace metals as well as their bioavailability in near-subsurface environments, including soils, sediments, and groundwater (Tesoriero and Pankow, 1996; Böttcher, 1998; Reeder et al., 1999; Lee et al., 2002; Lee et al., 2005a,b). The role of dissolved organic matter (DOM), a common component in many surficial aquatic environments, has become the focus of recent interest because of its potential influence on metal partitioning and other surface processes. Various types of organic species have been shown to sorb strongly at the calcite surface (Geffroy et al., 1999; Lee et al., 2005a), induce habit modification (Teng and Dove, 1997; Meldrum and Hyde, 2001; Orme et al., 2001), inhibit calcite precipitation (Inskeep and Bloom, 1986; Reddy and Hoch, 2001; Wada et al., 2001; Zuddas et al., 2003), and control the structural form of $CaCO_3$ precipitates (e.g., Manoli and Dalas, 2001; Manoli et al., 2002). Kitano et al. (1968) suggested that the cause of calcite growth inhibition could be related to the formation of aqueous calcium–DOM complexes, resulting in a decrease in the calcite saturation state of the growth solution. In contrast, most

* Corresponding author. Present address: Department of Geology and Geophysics, University of Wisconsin-Madison, 1215 W. Dayton St., Madison, WI 53706, USA. Fax: +1 608 262 0693.
E-mail address: yjlee@geology.wisc.edu (Y.J. Lee).

0016-7037/$ - see front matter © 2006 Elsevier Inc. All rights reserved.
doi:10.1016/j.gca.2006.01.025

subsequent workers have explained growth inhibition, as well as habit modification, by adsorption of organic species to the calcite surface, resulting in blockage of growth sites and reduced interfacial kinetics (e.g., Inskeep and Bloom, 1986; Reddy and Hoch, 2001; Wada et al., 2001; Zuddas et al., 2003).

In the present study, we examine the influence of two dissolved organic species—citrate and phthalate—on the coprecipitation of Co(II) with calcite. Previous studies have shown that calcite exhibits a high affinity for Co(II) incorporation during growth (Lorens, 1981; Reeder, 1996), substituting in the Ca site. Cobalt has also been the subject of interest because of its presence as a contaminant in aquatic and soil systems, where its occurrence may be attributed to industrial sources or, for example, to releases of high-level nuclear waste (e.g., Brooks and Herman, 1998; Brooks et al., 1998; Catalano et al., 2005). The increased mobility of Co in some near-subsurface environments has been attributed to the formation of Co–DOM complexes, with associated effects on Co sorption onto mineral surfaces (Jardine et al., 1993; Brooks et al., 1998). Zachara et al. (1994) and Brooks and Herman (1998) suggested that DOM can enhance Co sorption on subsurface materials through changes in the electrostatic properties of the mineral–water interface as well as through the formation of Co—organic ternary complexes at mineral surfaces. These studies imply that DOM may play an important role in controlling the uptake of these contaminants in subsurface environments.

In addition to the possible role of organic ligands, a variety of physicochemical parameters such as pH, solution composition, and precipitation rate have been demonstrated to influence partition coefficients for metal coprecipitating with calcite during crystallization. In organic-free systems, partition coefficients of transition and alkaline earth metals into calcite have been reported to be dependent on calcite precipitation rate. For example, divalent transition metals (e.g., Co, Mn, and Cd) are highly compatible with calcite ($K_d > 1$) and their partition coefficients decrease with increasing precipitation rate (Lorens, 1981; Tesoriero and Pankow, 1996). In contrast, the alkaline earth metals Mg, Sr, and Ba are incompatible ($K_d < 1$), and their partition coefficients increase with increasing precipitation rate (Lorens, 1981; Mucci and Morse, 1990; Morse and Bender, 1990; Rimstidt et al., 1998). As noted by many authors, this observation suggests that experimentally determined partition coefficients for these metals into calcite do not reflect equilibrium, and are influenced by kinetic and mechanistic factors. Furthermore, Paquette and Reeder (1995) and Reeder (1996) showed a correlation between structural aspects of growth steps and divalent metal incorporation into calcite. These studies indicate that Co incorporation into calcite is influenced by interfacial factors associated with calcite precipitation.

Relatively few studies have addressed metal coprecipitation with calcite in the presence of DOM. One of the more important findings from these studies is that metal–organic complexation in the parent solution may have an effect on metal incorporation into calcite (Kitano and Hood, 1965; Kitano et al., 1968). Kitano et al. (1968), for example, observed that zinc incorporation into calcite is controlled by DOM concentration, and concluded that the Zn partition coefficient in the presence of citrate is influenced by the formation of Zn–citrate complexes. This observation suggests that aqueous metal–organic speciation may be important in controlling metal coprecipitation with calcite. Nevertheless, not all organic species are expected to have a similar influence on metal uptake, and any effect would depend on the degree of complexation and the affinity of the complex for the surface. The fate of the organic species during coprecipitation has received little attention. Studies focusing on biomineralization have noted the presence of organic matter within calcite (Mann et al., 1993; Failini et al., 1996; Aizenberg et al., 1997; Addadi and Weiner, 2001). Hence it is important to know if metal–organic complexes or organic species undergo incorporation into calcite during crystallization.

In the present study, we examine the influence of the simple dissolved organic ligands citrate and phthalate on Co coprecipitation with calcite. There are several reasons for these choices of organic ligands. Both occur in near-surface aquatic systems. Citrate occurs naturally and as a contaminant, sometimes used in industrial applications because of its ability to form strong complexes with metals. Phthalates are widely used as softening agents in plastics, and may be introduced into water and soils as a result of leaching or from releases at manufacturing sites. These ligands exhibit different affinities for Co(II) in aqueous solution: Co binds more strongly to citrate than phthalate (Appendix Table A1). This difference reflects the different physicochemical properties of the ligands with regard to their molecular weight, structure (aliphatic chain vs. aromatic ring), arrangement of functional groups, hydrophilic vs. hydrophobic character, and acidity. Our experimental approach provides not only a systematic examination of Co partitioning as a function of calcite growth kinetics in the presence of dissolved citrate and phthalate, but also new insight into the behavior of these organic ligands during calcite crystallization.

2. Experimental procedures

2.1. Samples and preparation

A seeded constant-addition method was employed for Co coprecipitation experiments. By setting a fixed rate of addition of growth constituents to the batch-type reaction vessel, the growth solution evolved to a constant composition resulting in steady-state growth of calcite (e.g., Zhong and Mucci, 1993; Tesoriero and Pankow, 1996). Co partitioning was assessed after steady-state conditions were achieved. The initial growth solutions consisted of a

700 mL volume of 0.007 M $CaCl_2$–$NaHCO_3$ solution with 0.1 M NaCl as a background electrolyte. Co^{2+} from a $CoCl_2$ stock solution was added before the seeds were introduced into the reaction vessel to a concentration of 20 μM. A mass of 0.5 g of analytical reagent calcite (Alfa Aesar) with an average particle size of 5 μm ($0.2\ m^2\ g^{-1}$ BET surface area) was added to the reaction vessel. The initial growth solutions were oversaturated with respect to calcite (IAP/Ksp ≅ 12), with a pH approximately of 7.9. A steady-state solution composition was reached following the addition of (Ca,Co)Cl_2 and Na_2CO_3 solutions from separate syringes at precalibrated rates. Concentrations in the syringes were 10–100 mM ($CaCl_2$), 500 μM ($CoCl_2$), and 10–100 mM (Na_2CO_3). We were able to control the calcite precipitation rate by adjusting the solution concentrations in the syringes and the addition rate. The $CoCl_2$ was delivered with the $CaCl_2$ to account for loss from solution during growth, and the Co/Ca ratio was adjusted by trial-and-error so that near steady-state conditions could be achieved over time. Saturation states with respect to calcite during the steady-state period were within the range IAP/Ksp = 5.2–10.1 for low and high growth rates. Water-saturated air ($PCO_2 = 10^{-3.5}$ atm) was continuously bubbled through solutions, which were stirred using a Teflon floating stirbar throughout the entire coprecipitation. Growth solutions were undersaturated with respect to other potential solubility-limiting phases, such as sphaerocobaltite ($CoCO_3$) and cobalt hydroxide ($Co(OH)_2$).

Solutions for Co coprecipitation in the presence of dissolved organic acids differed only by addition of citric or phthalic acid into the (Ca,Co)Cl_2 syringe and the initial growth solution at concentrations of 500 and 20 μM, respectively. The latter concentration lies within the range of citrate concentrations observed in near-subsurface environments (e.g., Jardine et al., 1993; Brooks et al., 1998). The stock solution containing Co, Ca, and the organic acid for use as a titrant was prepared by first combining $CoCl_2$ and citrate (or phthalate) to give final concentrations of 500 μM for each. After storage in a refrigerator overnight, $CaCl_2$ and NaCl were added to give the desired concentrations. The pH was then adjusted to ~5.6 using NaOH or HCl.

At the end of the experiments, solids were filtered, rinsed repeatedly in deionized water, and dried at 60 °C. Rinsing is expected to have caused minor dissolution from the surface, however, this loss is insignificant relative to the mass precipitated during the experiments. XRD analysis of samples showed no indication of any secondary precipitate. Due to inherent limitations in sensitivity of this method, however, we cannot rule out the presence of a trace phase. Possible coprecipitation of citrate (or phthalate) with calcite during the experiments was investigated by Fourier-transform infra-red (FT-IR) spectroscopy and thermogravimetric analysis (TGA) of the precipitates. TGA was conducted in air at a heating rate of 5 °C min^{-1} from ambient temperature to 650 °C using a Netzsch STA 449C instrument.

2.2. Partition coefficients of Co into calcite

As pointed out above, one important goal in this study was to determine partition coefficients (K_d) of Co into calcite in the presence of dissolved organic ligands during steady-state conditions for calcite precipitation. Several properties of the growth solution were monitored to determine when the system reached steady-state conditions during an experiment. First, pH values of the growth solution were periodically monitored using a Ross electrode calibrated with NIST-traceable buffer solutions. Aliquots of the growth solution were periodically collected, filtered, and analyzed for [Ca] and [Co] using direct-coupled plasma (DCP) spectrometry. The total dissolved inorganic carbon (DIC) concentration was measured by a flow injection analysis system (FIA) (Hall and Aller, 1992). We concluded that a system reached steady-state conditions when all these properties reached values that remained constant within estimated uncertainties of measurements at a given syringe addition rate.

After each experiment reached a steady-state, the partition coefficient (K_d) was calculated using:

$$K_d = ([Co]/[Ca])_{solid}/([Co]/[Ca])_{soln}$$

where [Co] and [Ca] represent mole fractions in the solid and total molar concentrations in the growth solution. The moles of Co (or Ca) precipitated in the period of steady-state conditions were calculated from a mass balance of the precipitating solution:

$$Moles_{precip,T1\,to\,T2} = moles_{soln,T1} + moles_{added,T1\,to\,T2} - moles_{soln,T2}$$

where $moles_{soln,T1}$ is the number of moles of Co (or Ca) in the growth solution at the initial time of a steady-state condition, $moles_{added,T1\ to\ T2}$ is the number of moles of Co (or Ca) added into the reaction vessel by a syringe during the steady-state period, and $moles_{soln,T2}$ is the number of moles of Co (or Ca) remaining in the solution at the end of each experiment.

3. Results and discussion

3.1. Solution speciation

Aqueous speciation and saturation state were calculated using the program PHREEQC (Parkhurst and Appelo, 1999) with the Minteq v.4 database for Co-organic acid growth solutions as well as Co-only and citrate-only solutions. Relevant stability constants used in this database are given in Appendix Table A1. Solution compositions obtained during the final steady-state periods of the coprecipitation experiments were used for simulations. Speciation results for the intermediate growth rate (R = 30 μmol min^{-1} m^{-2}) experiments are given in Table 1. In these examples total Ca, DIC, Co, and citrate (or phthalate) concentrations were fixed at the steady state values of 4.8 mM, 2.3 mM, 40 μM, and 60 μM, respectively, with

Table 1
Aqueous speciation in Co(II), citrate, and phthalate growth solutions at pH 8.3

	Species (%)			
	Co(II) (only)	Citrate (only)	Citrate + Co(II)	Phthalate + Co(II)
Calcium species				
Ca^{2+}	97.85	96.71	96.79	97.71
Ca–citrate$^-$		1.16	1.08	
$CaHCO_3^+$	1.32	1.31	1.31	1.32
$CaCO_3^0$	0.83	0.82	0.82	0.83
Ca–phthalate				0.15
Cobalt species				
Co^{2+}	84.03		75.60	83.88
Co–citrate$^-$			10.01	
$CoCl^+$	7.34		6.61	7.32
$CoCO_3^0$	4.34		3.91	4.33
$CoHCO_3^+$	3.17		2.86	3.16
$CoOH^+$	1.02		0.92	1.02
$Co(OH)_2^0$	0.11		0.10	0.11
Co–phthalate				0.17
Citrate species				
Ca–citrate$^-$		92.73	86.55	
Citrate^{3-}		5.05	4.71	
Co–citrate$^-$			6.67	
Na-citrate^{2-}		2.04	1.90	
Phthalate species				
Phthalate^{2-}				69.77
Na-phthalate$^-$				18.17
Ca–phthalate				11.90
Co–phthalate				0.12

Note. Solution conditions correspond to steady-state growth period at $R = 30$ μmol min^{-1} m^{-2}: $[Ca(II)]_{total} = 4.8$ mM, $[Co(II)]_{total} = 40$ μM, $[Citrate]_{total} = 60$ μM, $[Phthalate]_{total} = 60$ μM, and DIC = 2.3 mM.

0.1 M NaCl as a background electrolyte at pH 8.3. The calculation indicates that ~97% of the calcium is present as aqueous Ca^{2+} in all solutions, with Ca–citrate (and Ca–phthalate) complexes being insignificant. In the citrate solutions, the dominant Co species is aqueous Co^{2+} (~75%), with the Co–citrate$^-$ complex accounting for ~10% of the total Co. The simulation also indicates that of the total citrate, the Ca–citrate$^-$ complex (87–92%) dominates over citrate^{3-} (~5%). In phthalate solutions, aqueous Co^{2+} (~84%) and phthalate^{2-} (~70%) are dominant species (Table 1).

Although citrate forms strong Ca–citrate complexes under the experimental conditions, these speciation calculations suggest that saturation state with respect to calcite is not significantly reduced by its presence because of the high Ca to ligand ratio of the growth solution.

3.2. Variations in solution composition in the absence and presence of citrate and phthalate for calcite precipitation experiments

To investigate the influence of the growth solution on Co coprecipitation with calcite and to determine the Co partition coefficients, aqueous [Ca] and [Co], pH, and DIC were measured for precipitation rates ranging from 3 to 300 μmol min^{-1} m^{-2} over durations ranging from 7 to 38 h, depending on the length of time required to reach steady-state conditions. The evolution of solution pH, [Ca], DIC, and [Co] are shown in Fig. 1 for intermediate and high precipitation rates of 30 and 300 μmol min^{-1} m^{-2}. Trends for other growth rates are not shown but exhibit similar behaviors. Solution pH in the absence and presence of citrate and phthalate increased initially and then maintained a relatively stable value (8.3–8.5) after a reaction time of 3–5 h (Figs. 1a and b). These observations are in good agreement with observations from a previous study (Zhong and Mucci, 1993), where solution pH became constant after a similarly short period. The evolution of aqueous [Ca] with and without dissolved organic ligands is shown in Figs. 1c and d. After a decrease in the initial 3–4 h of calcite precipitation in the absence of organic ligands, the aqueous [Ca] became nearly constant at ~4–5 mM, except in experiments with the lowest precipitation rate. The initially rapid decrease in [Ca] is most likely due to calcite precipitation upon the addition of the calcite seeds to the reactor. Zhong and Mucci (1993) reported similar observations in a study of calcite precipitation using a constant-addition technique.

The steady-state DIC over the experiment duration was found to be dependent on precipitation rate (Figs. 1e and f). At $R \geqslant 150$ μmol min^{-1} m^{-2}, only small differences were observed between experiments with and without organic ligands, with steady-state values reached after 3–4 h (Fig. 1e). At $R \leqslant 30$ μmol min^{-1} m^{-2}, however, DIC in the presence of dissolved organic ligands is higher than in experiments without organic ligands (Fig. 1f). All steady-state DIC values in experiments with and without dissolved organic ligands were nearly constant after 4 h.

The [Co] in the growth solution also decreased within the initial 4–5 h of the precipitation, but the decrease was found to be dependent on precipitation rate (Figs. 1g and h). For example, at $R = 300$ μmol min^{-1} m^{-2}, the initial ~20 μM Co decreased to ~10 μM by ~4 h, and then maintained a nearly constant value for the duration of the experiment. At $R = 30$ μmol min^{-1} m^{-2}, however, aqueous [Co] decreased slightly during the initial 1.5 h, then slowly increased in the following 6–10 h followed before reaching a steady-state. Only small differences were observed in the evolution of [Co] between systems with and without organic ligands. The constant values of aqueous [Co] in the growth solution during steady-state conditions indicate that Co coprecipitates with calcite rather than being removed by adsorption. If adsorption were responsible for the partitioning of the Co to calcite, aqueous [Co] should increase rather than leveling off during crystallization. Tesoriero and Pankow (1996) reported similar observations in a study of Cd coprecipitation with calcite, concluding that the constant value of [Cd] in a steady-state condition is consistent with incorporation of Cd into calcite.

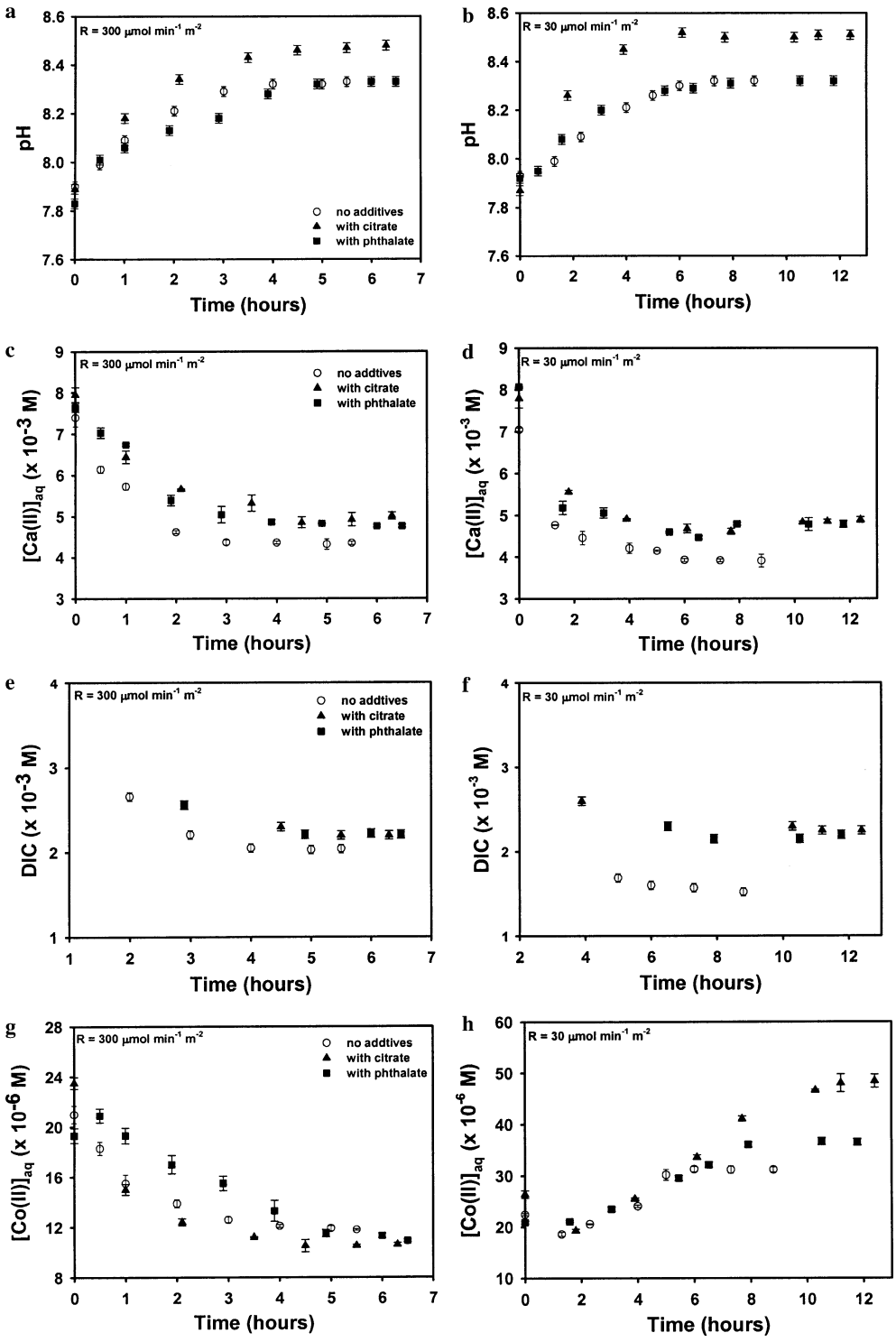

Fig. 1. Changes in (a,b) pH, (c,d) total Ca, (e,f) total dissolved inorganic carbon, and (g,h) total dissolved Co in calcite growth solutions as a function of time for calcite precipitation rates $R = 300$ and 30 μmol min^{-1} m^{-2}. See text for discussion.

3.3. Inhibition of calcite growth in the presence of citrate and phthalate

Although the differences are not large, there is a discernable effect of the presence of citrate and phthalate on the calcite growth kinetics relative to the organic-free systems. Fig. 2 shows the calcite growth rate as a function of calculated saturation index [SI = log(IAP/Ksp)] during the steady-state growth period for the organic-free and organic-containing systems. Although variability is clearly evident, the trends for phthalate- and citrate-containing systems are shifted to higher saturation states for comparable growth rate relative to the organic-free systems. This indicates that both organic ligands inhibit calcite precipita-

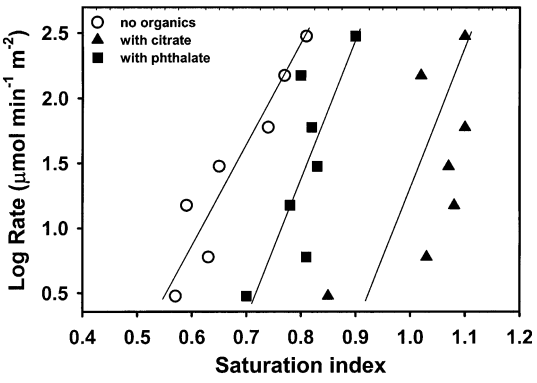

Fig. 2. Relationships between calcite saturation index [log(IAP/Ksp)] and growth rate for organic-free and organic-containing systems.

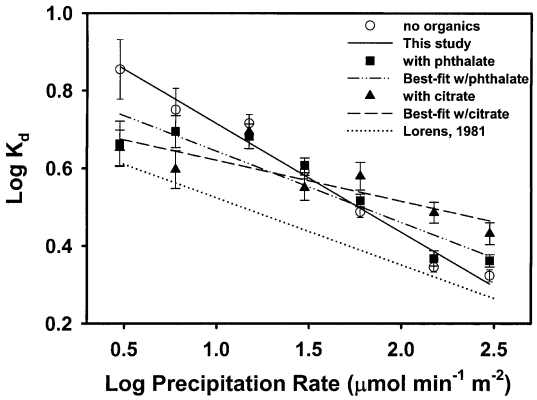

Fig. 3. Influence of precipitation rate on the partition coefficients for Co into calcite at room temperature in the absence and presence of dissolved organic acids, citrate and phthalate. Best-fit linear trends are shown. Error bars represent the standard deviations from triplicate measurements. The results from Lorens (1981) are shown for comparison.

tion, with a slightly great effect for citrate than for phthalate. Reddy and Hoch (2001) also observed that citrate exerted an inhibitory effect on calcite growth kinetics, although not as significant as for other polycarboxylic species. Growth inhibition is attributed to adsorption of the organic species at potential growth sites, thereby blocking attachment of Ca and/or CO_3 units (e.g., Inskeep and Bloom, 1986; Hoch et al., 2000). There is evidence that adsorption is most significant for species containing at least two carboxylate groups in a conformation that allows bidentate coordination to surface Ca atoms (Geffroy et al., 1999). These authors compared the sorption behavior of a range of carboxylic acids on calcite, including citrate and phthalate. Their results at pH 9 indicate that more citrate sorbs to the calcite surface than phthalate at equivalent concentrations. This may explain the greater inhibitory effect of citrate in our experiments.

3.4. Co coprecipitation with calcite in the absence and presence of citrate and phthalate

The Co partition coefficients in the absence and presence of citrate and phthalate as a function of calcite precipitation rate are shown in Fig. 3 and given in Table 2. These values correspond to steady-state conditions in the growth solutions. In organic-free systems, the partition coefficient decreases with increasing precipitation rate, following a nearly linear inverse correlation on a logarithmic plot. All of the partition coefficient values are greater than unity. The best-fit linear trend (Fig. 3) of the partition coefficients for the control system (no organic additives) lies slightly above the trend reported by Lorens (1981), and has a slightly greater slope. We note, however, that these results may not be directly comparable because different methods were used to determine surface areas. Lorens (1981) estimated surface area on the basis of SEM images, and we used BET gas adsorption.

The Co partition coefficients in phthalate and citrate systems also generally decrease with increasing calcite precipitation rate, although slightly greater deviations from linear trends are observed. K_d values were not found to be greatly different from those in the organic-free system at comparable precipitation rates. Best-fit linear trends in phthalate and citrate systems exhibit slightly lower slopes than the organic-free trend, although deviations at the lowest precipitation rates account for much of this difference. An analysis of covariance among the three datasets shows that the best-fit lines for the phthalate and citrate data fall just outside the 95% confidence interval of the best-fit line for the organic-free control data. Phthalate and citrate lines lie within each other's 95% confidence interval. Therefore, the differences in slope of the phthalate and citrate trends relative to the control are statistically significant. However, the differences are small, and hence we conclude that other factors, such as solution composition, precipitation rate, and interfacial kinetics, are likely to remain the primary factors controlling the K_d behavior of Co with calcite.

3.5. Citrate incorporation into calcite during crystallization

TGA and FT-IR spectroscopy were used to investigate possible incorporation of phthalate and citrate into calcite during Co coprecipitation. TGA weight-loss curves for various seeded coprecipitates and a control sample are shown in Fig. 4. The control sample (calcite seed + pure overgrowth) was grown identically to the Co-, citrate-, and phthalate-containing calcite samples, except for the absence of these coprecipitates. Because CO_2 loss for calcite occurs at 700–800 °C in air (Sanders and Gallagher, 2002; Bertram and Klimm, 2004; see Fig. 4 inset), TGA was conducted up to 650 °C. All samples show minor loss of surface water below 375 °C. With TGA limited to $T < 650$ °C, the only significant mass loss for the control sample occurs at 475–550 °C. The weight-loss curve for an organic-free Co–calcite coprecipitate is essentially the same as for the control sample. The weight-loss curve for the Co–phthalate coprecipitate is also indistinguishable from those for the control sample and the organic-free Co coprecipitate.

Table 2
Partition coefficients of Co(II) coprecipitation with calcite in the absence and presence of citrate and phthalate

Experiment	Organic	pH[a]	Duration[b] (h)	log R (μmol min^{-1} m^{-2})	log K_d[c]	$(Co/Ca)_{aq}$[c]
CoCCcoppt01	NA	8.25	36.6	0.477	0.855	8.65
CoCCcoppt03	NA	8.29	11.2	0.778	0.751	12.1
CoCCcoppt07	NA	8.32	32.0	1.176	0.716	6.60
CoCCcoppt09	NA	8.32	8.8	1.477	0.593	7.96
CoCCcoppt13	NA	8.30	8.0	1.778	0.488	9.60
CoCCcoppt17	NA	8.32	6.7	2.176	0.345	2.52
CoCCcoppt23	NA	8.33	5.5	2.477	0.323	2.75
CoCCcoppt25	Citrate	8.35	38.0	0.477	0.653	8.35
CoCCcoppt28	Citrate	8.48	7.3	0.778	0.597	7.18
CoCCcoppt35	Citrate	8.52	52.3	1.176	0.694	7.40
CoCCcoppt39	Citrate	8.51	12.4	1.477	0.550	9.89
CoCCcoppt45	Citrate	8.47	6.8	1.778	0.580	10.1
CoCCcoppt49	Citrate	8.46	7.3	2.176	0.486	1.85
CoCCcoppt55	Citrate	8.48	6.3	2.477	0.432	2.12
CoCCcoppt62	Phthalate	8.23	37.0	0.477	0.663	9.01
CoCCcoppt65	Phthalate	8.30	8.3	0.778	0.695	7.17
CoCCcoppt70	Phthalate	8.34	46.3	1.176	0.683	6.57
CoCCcoppt75	Phthalate	8.32	11.8	1.477	0.608	7.85
CoCCcoppt79	Phthalate	8.32	8.2	1.778	0.517	7.70
CoCCcoppt83	Phthalate	8.32	11.3	2.176	0.368	2.50
CoCCcoppt89	Phthalate	8.34	6.5	2.477	0.362	2.60

[a] Measured at steady-state conditions.
[b] Duration of experiment.
[c] Calculated at steady-state conditions.

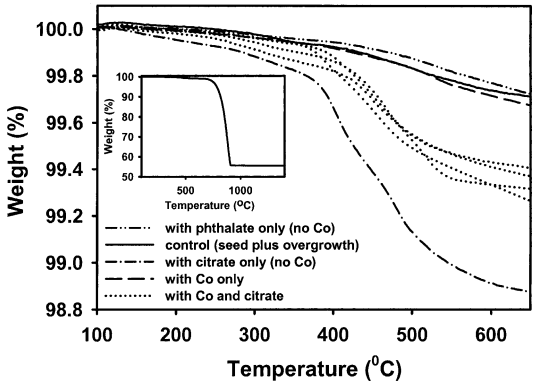

Fig. 4. TGA weight-loss curves from 100 to 650 °C for calcite coprecipitates with Co, Co–citrate, and Co–phthalate, and a calcite control (calcite seed + pure overgrowth). The inset plot shows weight loss up to 1400 °C, in which the large decrease over the range 700–900 °C corresponds to CO_2 loss.

In contrast, the TGA curves for samples coprecipitated with citrate (Fig. 4) show a more significant mass loss between 375 and 550 °C. The weight-loss curves for four different Co–citrate coprecipitates are all similar (dotted lines in Fig. 4), with slightly more than 0.5% total weight loss. Also shown in Fig. 4 is the weight-loss curve for a citrate-only coprecipitate, which was grown identically to the Co–citrate coprecipitates but in the absence of Co. This curve reveals a slightly greater weight loss between 375 and 550 °C, with approximately 1% total loss.

Several studies have demonstrated that the decomposition of organic ligands, particularly citrate trapped in the bulk of solids, begins at 350 °C and continues up to ~600 °C (e.g., Thongtem and Thongtem, 2004; Guo et al., 2004). The similarity of our results with these prior studies suggests that the mass loss at 375–550 °C is attributable to the breakdown of citrate incorporated in the calcite during crystallization. This is unlikely to represent citrate bound at the calcite surface because we extensively rinsed samples prior to TGA. Consequently, we conclude that some citrate is coprecipitated with calcite whereas phthalate is not to any discernable extent.

In a separate study using NMR spectroscopy, Phillips et al. (2005) examined the same citrate-only coprecipitate described above. Their $^{13}C\{^1H\}$ CP-MAS NMR observations confirmed the incorporation of ~1 wt% citrate into the bulk structure, as demonstrated by polarization transfer between citrate and bulk structural carbonate groups. They also found that water molecules are associated with the citrate, and suggested that they may be involved in accommodation of the molecule in the calcite structure. In contrast, they found no evidence for incorporation of phthalate. These NMR findings raise the possibility that the observed weight loss between 375 and 550 °C may reflect not only the breakdown of citrate but also the release of associated water. FT-IR spectra described below provide additional evidence for the presence of water in the Co–citrate coprecipitates. We note that the estimate of ~1 wt% citrate based on the NMR observation is approximately the same as indicated by the TGA weight loss (Fig. 4).

FT-IR spectra of the Co–calcite coprecipitates in the presence of citrate and phthalate are shown in Fig. 5. The FT-IR spectra of the calcite seed and the control

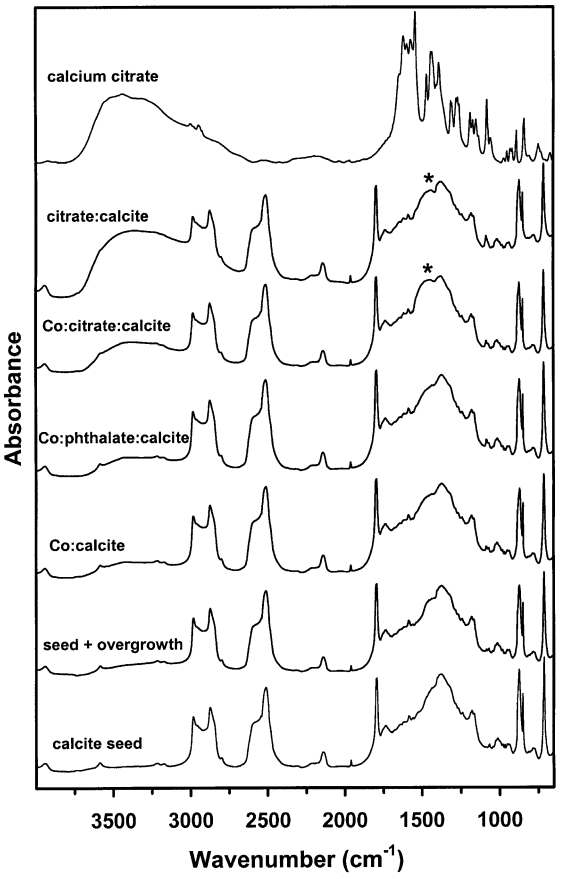

Fig. 5. FT-IR spectra of the calcite seed, calcite control (seed + pure overgrowth), Co(II)-organic-calcite coprecipitates, and calcium citrate tetrahydrate samples. Weak feature indicated by * is described in the text.

(calcite seed + pure overgrowth) are identical and consistent with previously reported spectra for pure calcite (White, 1974; Balmain et al., 1999; Cebeci and Sönmez, 2004). No bands attributable to other mineral phases (including other $CaCO_3$ polymorphs) or organic acids are observed. The absence of other mineral phases is supported by our XRD results (data not shown). The spectra for the Co–calcite and Co–phthalate–calcite coprecipitates (Fig. 5) are also indistinguishable from the calcite seed and control spectra, whereas the spectra for the Co–citrate–calcite and citrate–calcite coprecipitates exhibit at least two noticeable differences. A very broad, diffuse absorption is evident over the region 3700–3100 cm^{-1} in the Co–citrate–calcite and citrate-calcite spectra. This broad feature is almost certainly attributable to stretching modes of structural water (e.g., Balmain et al., 1999; Cebeci and Sönmez, 2004). A similar broad absorption due to structural water is evident in the FT-IR spectrum of calcium citrate tetrahydrate, which is shown for comparison in Fig. 5. Hence, the presence of this broad feature in the two citrate-containing calcite samples and its absence in the seed, control, and phthalate samples likely reflect the presence of water associated with the citrate, as concluded by Phillips et al. (2005).

It is notable that the spectra for the two citrate-calcite coprecipitates exhibit no sharp absorption bands that correspond to those seen in the calcium citrate spectrum even though a small amount of citrate is known to be present on the basis of TGA and NMR. The most probable explanation for the absence of characteristic absorption features is the low concentration of citrate present (0.5–1 wt%), which is likely to be below detection. We note, however, that the two citrate-calcite spectra exhibit a weak shoulder at 1550–1430 cm^{-1} (indicated by * in Fig. 5), which is not present in any of the other calcite spectra. There is insufficient information for us to assign this subtle feature to citrate, even though it does correspond to the position of stretching modes typical of carboxylates near 1670–1540 and 1420–1200 cm^{-1}. Several studies have demonstrated that the positions of these stretching modes are sensitive to protonation and binding to metal ions (e.g., Cabaniss and McVey, 1995; Strathmann and Myneni, 2004).

Whereas the TGA and FT-IR results are consistent with the incorporation of citrate and associated water into calcite during growth, there is no evidence of phthalate incorporation under similar experimental conditions. On the basis of the aqueous speciation (Table 1), we propose that citrate is incorporated as the Ca–citrate complex. In citrate solutions, this species accounts for ~87–93% of the total citrate, with free $citrate^{3-}$ making up ~5% (Table 1), whereas in phthalate solutions, the Ca–phthalate species is less than 12% of the total phthalate, with free phthalate accounting for ~70%. We also note that the Co–citrate complex is noticeably more abundant than the Co–phthalate complex in comparable coprecipitation solutions, but we do not consider this difference to be responsible for the differential incorporation of citrate and phthalate. In the Co-free, citrate-containing solution (Table 1), the Co–citrate complex is obviously absent, yet the TGA results showed greater citrate incorporation than when both Co and citrate are present in solution. This is consistent with our hypothesis that the $Ca–citrate^{-}$ species is involved in the incorporation. Accordingly, we deduce that free $citrate^{3-}$, which is significantly less abundant in both citrate solutions than free $phthalate^{2-}$ is in the phthalate solution, is unlikely to be directly involved in the incorporation.

Aqueous speciation alone may not explain the incorporation of citrate and apparent exclusion of phthalate. It is also important to recognize the different structures of these two organic ligands and the stereochemistry of their carboxylate groups. Over the pH range of the experiments (7.9–8.5), the carboxyl groups of both citric and phthalic acids are fully deprotonated ($pK_{a3} = 6.4$ for citric acid; $pK_{a2} = 5.4$ for *o*-phthalic acid). Phthalate has two *ortho*-positioned carboxylate groups on an aromatic ring (Fig. 6a), whereas citrate has an aliphatic structure with three carboxylate groups separated by 2–3 carbon atoms (Fig. 6b). Above, we inferred that the Ca–citrate complex has a strong affinity for the calcite surface and is readily incorporated during precipitation. An X-ray structural study of the 1:1 calcium citrate trihydrate shows that Ca

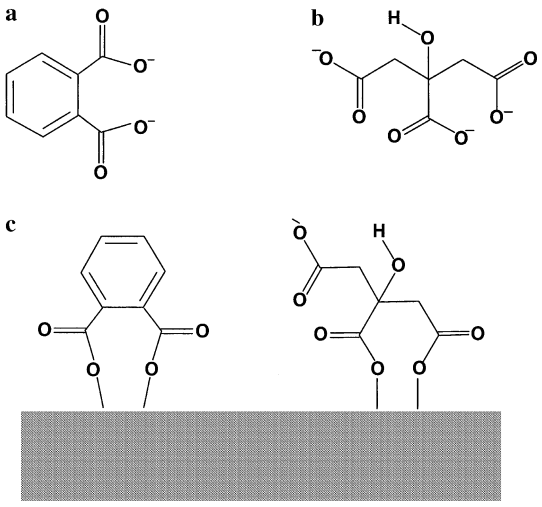

Fig. 6. Schematic illustrations of (a) phthalate and (b) citrate ligands, and (c) hypothetical models illustrating their sorption at the calcite surface. Once the carboxylate groups of phthalate (left) are committed to the surface, the exposed aromatic ring is hydrophobic and does not allow further attachment of growth units. Although only one of several possible modes of citrate binding is shown (right), carboxylate or hydroxyl groups not committed to the surface are available for attachment of Ca, allowing continued growth.

binds with citrate in a bidentate fashion involving two carboxylate groups or a carboxylate group and a hydroxyl oxygen (Sheldrick, 1974). Glusker (1980) noted, however, that metal coordination by citrate may be monodentate, bidentate, or tridentate, and may involve any of the carboxylate groups and the hydroxyl. Geffroy et al. (1999) examined the sorption of various carboxylates at the calcite surface, and inferred that, in general, two carboxylate groups coordinate to a surface Ca but, in cases where an α-hydroxycarboxylate is present, as in citrate, coordination by a carboxylate and the hydroxyl oxygen may be favored. Nevertheless, there may not be a unique mode of citrate sorption at the calcite surface. The observation by Phillips et al. (2005) of broad peaks in $^{13}C\{^{1}H\}$ CP-MAS NMR spectra from calcite coprecipitated with citrate indicates multiple conformations of citrate within the calcite. Different modes of binding may also occur at the surface.

Although we do not know its exact conformation, it appears reasonable to infer that a Ca coordinates with citrate in a bidentate, or possibly tridentate, linkage, and this complex sorbs to the calcite surface, reflecting the affinity of carboxylate groups for surface Ca atoms or the affinity of the calcite surface for the partially coordinated Ca in the Ca–citrate complex. Regardless of the exact coordination of the citrate at the surface, uncoordinated carboxylate and/or hydroxyl group(s) exhibit a hydrophilic character and are potential sites of Ca attachment and further $CaCO_3$ growth. Fig. 6c shows a purely hypothetical example of citrate attachment at the calcite surface. Because of the position and spacing of carboxylate groups around the chain, further attachment of Ca to citrate is possible after it sorbs. Additionally, hydrogen-bonded interactions involving H_2O (or OH^-) are possible, which Phillips et al. (2005) noted were likely to be required to accommodate the citrate in the calcite structure. The stereochemistry of the carboxylate groups may be the principal factor that facilitates citrate incorporation during growth. Other workers have emphasized the importance of positioning of functional groups for addition of Ca and CO_3^{2-} for calcite growth (cf. Mann et al., 1993). Phillips et al. (2005) noted that the C1–C5 carboxylate distance in citrate (5.1 Å) is similar to the 4.99 Å Ca–Ca (and CO_3–CO_3) spacing along the calcite cleavage edge.

The *ortho*-position of the two carboxylate groups around the aromatic ring in phthalate presents a very different situation. Phthalate does not complex significantly with Ca in solution, which suggests a lower affinity for binding at surface Ca sites. Studies of phthalate sorption on other mineral sorbents have suggested that inner- and outer-sphere adsorption surface complexes may occur, depending on solution factors, such as pH and ionic strength (Boily et al., 2000). If phthalate sorbs as an inner-sphere surface complex, with the two carboxylate groups associated with a surface Ca atom, the aromatic ring would present a hydrophobic character with no sites for further attachment of either Ca or CO_3. Without further possibility of attachment of growth units, phthalate incorporation may not be favored. Consequently, sorbed phthalate may need to desorb before further growth of calcite can occur. If outer-sphere sorption occurs, then the low affinity of phthalate for Ca also suggests that it is unlikely to be incorporated and is more likely to be desorbed prior to further growth of calcite. These arguments for preferential incorporation of citrate and exclusion of phthalate remain speculative, but suggest a model for further testing.

The preferential incorporation of citrate over phthalate may provide insight to the principal factors that control incorporation of macromolecules into the calcium carbonate structure during biomineralization. The presence of citrate may influence crystal growth, morphology, and mechanical properties of the host calcite. Furthermore, the involvement of water molecules associated with citrate incorporation may play a key role in accommodating a large guest molecule within the calcite structure. Additional work is needed to address these aspects as well as the long-term stability of these coprecipitates.

4. Summary

The findings of this study suggest that dissolved citrate and phthalate, over the range of concentrations investigated, have little influence on the partitioning behavior of Co into calcite under steady-state growth conditions. Only small differences are observed in the K_d trends with and without these organic ligands as a function of calcite precipitation rate, except at very low rates. Consequently it is likely that the interaction of the metal (i.e., Co^{2+}) at the calcite–water interface, rather

than the metal-organic complex, is primarily responsible for the incorporation behavior of Co. It remains to be determined if other metals and organic species will behave similarly. Our findings show that calcite precipitation is slightly inhibited by these organic ligands at the concentrations used in this study. Because of the high Ca to ligand ratio of the growth solutions, calcite supersaturation is not significantly affected by the presence of citrate or phthalate and, thus, inhibition is attributed to adsorption of the organics at the surface and interference with growth sites.

TGA curves for citrate-calcite coprecipitates in the absence and presence of Co show a significant (i.e., 0.5–1 wt%) mass loss between 350 and 600 °C, which is attributed to the decomposition of citrate in the calcite structure, suggesting citrate incorporation into calcite during crystallization. The TGA curves, however, reveal no difference between samples with and without phthalate, suggesting no incorporation of phthalate into calcite. Aqueous speciation calculations indicate that citrate occurs predominantly as Ca–citrate complexes, whereas phthalate remains largely uncomplexed. These results imply that changes such as the formation of aqueous metal–organic complexes in the growth solution may be one important factor accounting for organic coprecipitation with calcite during crystallization. Functionality of the organic ligands may also play a role. FT-IR spectra indicate that structural water is present in citrate-containing calcite.

The findings of this study demonstrate that dissolved organic molecules can be incorporated in calcite in concentrations up to ~1 wt%, but the incorporation depends on the functionality and complexation of the organic ligand. One implication of this study is that organic ligands associated with the biologically mediated growth of calcite may be included in the structure, thereby affecting its composition, solubility, and other properties. It remains to be determined if dissolved metal–organic complexes may be coprecipitated with calcite during crystallization.

Acknowledgments

Funding for this work was provided by NSF grant CHE 0221934 through the Center for Environmental Molecular Science. We thank Xianzhong Guo for assistance with TGA data collection, and Brian Phillips and Evert Elzinga for useful discussions. Comments from two anonymous reviewers and Associate Editor Alfonso Mucci improved the manuscript significantly.

Associate editor: Alfonso Mucci

Appendix A

See Table A1.

Table A1
Stability constants (log K) used for aqueous Ca^{2+}, Co^{2+}, citrate, phthalate, and their complex speciation calculation

	log K
$Co^{2+} + H_2O = CoOH^+ + H^+$	−9.697
$Co^{2+} + 2H_2O = Co(OH)_2{}^0 + 2H^+$	−18.794
$Co^{2+} + 3H_2O = Co(OH)_3{}^- + 3H^+$	−31.491
$Co^{2+} + 4H_2O = Co(OH)_4{}^{2-} + 4H^+$	−46.288
$2Co^{2+} + H_2O = Co_2OH^{3+} + H^+$	−10.997
$4Co^{2+} + 4H_2O = Co_4(OH)_4^{4+} + 4H^+$	−30.488
$Co^{2+} + 2H_2O = CoOOH^- + 3H^+$	−32.092
$Co^{2+} + CO_3{}^{2-} = CoCO_3{}^0$	4.228
$Co^{2+} + H^+ + CO_3{}^{2-} = CoHCO_3{}^+$	12.220
$H^+ + Citrate^{3-} = H(Citrate)^{2-}$	6.396
$2H^+ + Citrate^{3-} = H_2(Citrate)^-$	11.157
$3H^+ + Citrate^{3-} = H_3(Citrate)^0$	14.285
$Ca^{2+} + Citrate^{3-} = Ca(Citrate)^-$	4.870
$Ca^{2+} + Citrate^{3-} + H^+ = CaH(Citrate)^0$	9.260
$Ca^{2+} + Citrate^{3-} + 2H^+ = CaH_2(Citrate)^+$	12.257
$Co^{2+} + Citrate^{3-} = Co(Citrate)^-$	6.187
$Co^{2+} + H^+ + Citrate^{3-} = CoH(Citrate)^0$	10.444
$Co^{2+} + 2H^+ + Citrate^{3-} = CoH_2(Citrate)^+$	12.786
$Na^+ + Citrate^{3-} = Na(Citrate)^{2-}$	1.030
$2Na^+ + Citrate^{3-} = Na_2(Citrate)^-$	1.500
$Na^+ + Citrate^{3-} + H^+ = NaH(Citrate)^-$	6.450
$H^+ + Phthalate^{2-} = H(Phthalate)^-$	5.408
$2H^+ + Phthalate^{2-} = H_2(Phthalate)^0$	8.358
$Ca^{2+} + Phthalate^{2-} = Ca(Phthalate)^0$	2.450
$Ca^{2+} + Phthalate^{2-} + H^+ = CaH(Phthalate)^+$	6.430
$Co^{2+} + Phthalate^{2-} = Co(Phthalate)^0$	2.830
$Co^{2+} + H^+ + Phthalate^{2-} = CoH(Phthalate)^+$	7.227
$Na^+ + Phthalate^{2-} = Na(Phthalate)^-$	0.800

National Institute of Standards and Technology (NIST) database as given in PHREEQC with minteq.v4.dat database (2005). Log K values given for infinite dilution scale and 25 °C.

References

Addadi, L., Weiner, S., 2001. Biomineralization: crystals, asymmetry and life. *Nature* **411**, 753–755.

Aizenberg, J., Hanson, J., Koetzle, T.F., Weiner, S., Addadi, L., 1997. Control of macromolecule distribution within synthetic and biogenic single calcite crystals. *J. Am. Chem. Soc.* **119**, 881–886.

Balmain, J., Hannoyer, B., Lopez, E., 1999. Fourier transform infrared spectroscopy (FTIR) and X-ray diffraction analyses of mineral and organic matrix during heating of mother of pearl (nacre) from the shell of the Mollusc *Pinctada maxima*. *J. Biomed. Mater. Res.* **48**, 749–754.

Bertram, R., Klimm, D., 2004. Assay measurements of oxide materials by thermogravimetry and ICP-OES. *Thermochim. Acta* **419**, 189–193.

Boily, J.F., Nilsson, N., Persson, P., Sjoeberg, S., 2000. Benzenecarboxylate surface complexation at the goethite (α-FeOOH)/water interface: I. A mechanistic description of pyromellitate surface complexes from the combined evidence of infrared spectroscopy, potentiometry, adsorption data, and surface complexation modeling. *Langmuir* **16**, 5719–5729.

Böttcher, M., 1998. Manganese(II) partitioning during experimental precipitation of rhodochrosite-calcite solid solution from aqueous solutions. *Mar. Chem.* **62**, 287–297.

Brooks, S.C., Herman, J.S., 1998. Rate and extent of cobalt sorption to representative aquifer minerals in the presence of a moderately strong organic ligand. *Appl. Geochem.* **13**, 77–88.

Brooks, S.C., Herman, J.S., Hornberger, G.M., Mills, A.L., 1998. Biodegradation of cobalt–citrate complexes: implications for cobalt mobility in ground water. *J. Contam. Hydrol.* **32**, 99–115.

Cabaniss, S.E., McVey, I.F., 1995. Aqueous infrared carboxylate absorbances: Aliphatic monocarboxylates. *Spectrochim. Acta, Part A* **51**, 2385–2395.

Catalano, J.G., Warner, J.A., Brown, G.E., 2005. Sorption and precipitation of Co(II) in Hanford sediments and alkaline aluminate solutions. *Appl. Geochem.* **20**, 193–205.

Cebeci, Y., Sönmez, I., 2004. A study on the relationship between critical surface tension of wetting and oil agglomeration recovery of calcite. *J. Colloid Interface Sci.* **273**, 300–305.

Curti, E., 1999. Coprecipitation of radionuclides with calcite: estimation of partition coefficients based on a review of laboratory investigations and geochemical data. *Appl. Geochem.* **14**, 433–445.

Failini, G., Albeck, S., Weiner, S., Addadi, L., 1996. Control of aragonite or calcite polymorphism by mollusk shell macromolecules. *Science* **271**, 67–69.

Geffroy, C., Foissy, A., Persello, J., Cabane, B., 1999. Surface complexation of calcite by carboxylates in water. *J. Colloid Interface Sci.* **211**, 45–53.

Glusker, J.P., 1980. Citrate conformation and chelation: enzymatic implications. *Acc. Chem. Res.* **13**, 345–352.

Guo, X., Sujatha, D.P., Ravi, B.G., John, P.B., Sanjay, S., Hanson, J.C., 2004. Phase evolution of yttrium aluminium garnet (YAG) in a citrate-nitrate gel combustion process. *J. Mater. Chem.* **14**, 1288–1292.

Hall, O.J., Aller, R.C., 1992. Rapid, small-volume, flow injection analysis for ΣCO_2 and NH_4^+ in marine and freshwaters. *Limnol. Oceanogr.* **37**, 1113–1119.

Hoch, A.R., Reddy, M.M., Aiken, G.R., 2000. Calcite crystal growth inhibition by humic substances with emphasis on hydrophobic acids from the Florida Everglades. *Geochim. Cosmochim. Acta* **64**, 61–72.

Inskeep, W.P., Bloom, P.R., 1986. Kinetics of calcite precipitation in the presence of water-soluble organic ligands. *Soil Sci. Soc. Am. J.* **50**, 1167–1172.

Jardine, P.M., Jacobs, G.K., O'Dell, J.D., 1993. Unsaturated transport processes in undisturbed heterogeneous porous media: II Co-contaminants. *Soil Sci. Soc. Am. J.* **57**, 954–962.

Kitano, Y., Hood, D.W., 1965. The influence of organic material on the polymorphic crystallization of calcium carbonate. *Geochim. Cosmochim. Acta* **29**, 29–41.

Kitano, Y., Tokuyama, A., Kanamori, N., 1968. Measurement of the distribution coefficient of zinc and copper between carbonate precipitation and solution. *J. Earth Sci., Nagoya Univ.* **16**, 1–50.

Lee, Y.J., Reeder, R.J., Wenskus, R.W., Elzinga, E.J., 2002. Structural relaxation in the $MnCO_3$–$CaCO_3$ solid solution: a Mn K-edge EXAFS study. *Phys. Chem. Miner.* **29**, 585–594.

Lee, Y.J., Elzinga, E.J., Reeder, R.J., 2005a. Cu(II) adsorption at the calcite–water interface in the presence of natural organic matter: kinetic studies and molecular-scale characterization. *Geochim. Cosmochim. Acta* **69**, 49–61.

Lee, Y.J., Elzinga, E.J., Reeder, R.J., 2005b. Sorption mechanisms of zinc on hydroxyapatite: systematic uptake studies and EXAFS spectroscopy analysis. *Environ. Sci. Technol.* **39**, 4042–4048.

Lorens, R.B., 1981. Sr, Cd, Mn, and Co distribution coefficients in calcite as a function of calcite precipitation rate. *Geochim. Cosmochim. Acta* **45**, 553–561.

Mann, S., Archibald, D.D., Didymus, J.M., Douglas, T., Heywood, B.R., Meldrum, F.C., Reeves, N.J., 1993. Crystallization at inorganic-organic interfaces: biominerals and biomimetic synthesis. *Science* **261**, 1286–1292.

Manoli, F., Dalas, E., 2001. Calcium carbonate crystallization in the presence of glutamic acid. *J. Cryst. Growth* **222**, 293–297.

Manoli, F., Kanakis, J., Malkaj, P., Dalas, E., 2002. The effect of aminoacids on the crystal growth of calcium carbonate. *J. Cryst. Growth* **236**, 363–370.

Meldrum, F.C., Hyde, S.T., 2001. Morphological influence of magnesium and organic additives on the precipitation of calcite. *J. Cryst. Growth* **231**, 544–558.

National Institute of Standards and Technology (NIST) thermochemical database 46 version 7, 2003.

Morse, J.W., Bender, M.L., 1990. Partition coefficients in calcite: examination of factors influencing the validity of experimental results and their application to natural systems. *Chem. Geol.* **82**, 265–277.

Mucci, A., Morse, J.W., 1990. Chemistry of low-temperature abiotic calcites: experimental studies on coprecipitation, stability and fractionation. *Aquatic Sci.* **3**, 217–254.

Orme, C.A., Noy, A., Wierzbicki, A., McBride, M.T., Grantham, M., Teng, H., Dove, P.M., De Yoreo, J.J., 2001. Formation of chiral morphologies through selective binding of amino acids to calcite surface steps. *Nature* **411**, 775–779.

Paquette, J., Reeder, R.J., 1995. Relationship between surface structure, growth mechanism, and trace element incorporation in calcite. *Geochim. Cosmochim. Acta* **59**, 735–749.

Parkhurst, D.L., Appelo, C.A.J., 1999. User's guide to PHREEQC (Version 2)—A computer program for speciation, batch-reaction, one-dimensional transport, and inverse geochemical calculations: U.S. Geological Survey Water-Resources Investigations Report 99-4259, 310 p.

Phillips, B.L., Lee, Y.J., Reeder, R.J., 2005. An NMR spectroscopic study of organic coprecipitates in calcite. *Environ. Sci. Technol.* **39**, 4533–4539.

Reddy, M.M., Hoch, A.R., 2001. Calcite crystal growth rate inhibition by polycarboxylic acids. *J. Colloid Interface Sci.* **235**, 365–370.

Reeder, R.J., 1996. Interaction of divalent cobalt, zinc, cadmium, and barium with the calcite surface during layer growth. *Geochim. Cosmochim. Acta* **60**, 1543–1552.

Reeder, R.J., Lamble, G.M., Northrup, P.A., 1999. XAFS study of the coordination and local relaxation around Co^{2+}, Zn^{2+}, Pb^{2+}, and Ba^{2+} trace elements. *Am. Miner.* **84**, 1049–1060.

Rimstidt, J.D., Balog, A., Webb, J., 1998. Distribution of trace elements between carbonate minerals and aqueous solutions. *Geochim. Cosmochim. Acta* **62**, 1851–1863.

Sanders, J.P., Gallagher, P.K., 2002. Kinetic analyses using simultaneous TG/DSC measurements Part I: decomposition of calcium carbonate in argon. *Thermochim. Acta* **388**, 115–128.

Sheldrick, B., 1974. Calcium hydrogen citrate trihydrate. *Acta Crystallogr. B* **30**, 2056–2057.

Strathmann, T.J., Myneni, S.C.B., 2004. Speciation of aqueous Ni(II)-carboxylate and Ni(II)-fulvic acid solutions: combined ATR-FTIR and XAFS analysis. *Geochim. Cosmochim. Acta* **68**, 3441–3458.

Teng, H.H., Dove, P.M., 1997. Surface site-specific interactions of aspartate with calcite during dissolution: Implications for biomineralization. *Am. Miner.* **82**, 878–887.

Tesoriero, A., Pankow, J., 1996. Solid solution partitioning of Sr^{2+}, Ba^{2+} and Cd^{2+} to calcite. *Geochim. Cosmochim. Acta* **60**, 1053–1063.

Thongtem, T., Thongtem, S., 2004. Characterization of Bi4Ti3O12 powder prepared by the citrate and oxalate coprecipitation processes. *Ceram. Int.* **30**, 1463–1470.

Wada, N., Kanamura, K., Umegaki, T., 2001. Effects of carboxylic acids on the crystallization of calcium carbonate. *J. Colloid Interface Sci.* **233**, 65–72.

White, W.B., 1974. The carbonate minerals. In: Farmer, V.C. (Ed.), *The Infrared Spectra of Minerals*. Mineralogical Society, pp. 227–284.

Zachara, J.M., Resch, C.T., Smith, S.C., 1994. Influence of humic substances on Co^{2+} sorption by a subsurface mineral separate and its mineralogic components. *Geochim. Cosmochim. Acta* **58**, 553–566.

Zhong, S., Mucci, A., 1993. Calcite precipitation in seawater using a constant addition technique: a new overall reaction kinetic expression. *Geochim. Cosmochim. Acta* **57**, 1409–1417.

Zuddas, P., Pachana, K., Faivre, D., 2003. The influence of dissolved humic acids on the kinetics of calcite precipitation from seawater solutions. *Chem. Geol.* **201**, 91–101.